

A Divide-and-Conquer Approach to Dicke State Preparation*

Shamminuj Aktar^{1,2,*}, Andreas Bärttschi^{2,*},
Abdel-Hameed A. Badawy¹, Stephan Eidenbenz²

¹ Klipsch School of Electrical and Computer Engineering, New Mexico State University

² CCS-3 Information Sciences, Los Alamos National Laboratory

Abstract

We present a divide-and-conquer approach to deterministically prepare Dicke states $|D_k^n\rangle$ (i.e., equal-weight superpositions of all n -qubit states with Hamming Weight k) on quantum computers. In an experimental evaluation for up to $n = 6$ qubits on IBM Quantum Sydney and Montreal devices, we achieve significantly higher state fidelity compared to previous results [26, Mukherjee et.al. TQE'2020], [10, Cruz et.al. QuTe'2019].

The fidelity gains are achieved through several techniques: Our circuits first “divide” the Hamming weight between blocks of $n/2$ qubits, and then “conquer” those blocks with improved versions of Dicke state unitaries [3, Bärttschi et.al. FCT'2019]. Due to the sparse connectivity on IBM’s heavy-hex-architectures, these circuits are implemented for linear nearest neighbor topologies. Further gains in (estimating) the state fidelity are due to our use of measurement error mitigation and hardware progress.

1 Introduction

In quantum computing, Dicke states [12] are a class of highly-entangled quantum states with the rare feature that they are of importance as initial states in quantum algorithms, in addition to their quantum mechanical property of being highly entangled. The Dicke state $|D_k^n\rangle$ assigns equal non-zero amplitudes of $1/\sqrt{\binom{n}{k}}$ to each computational basis state of Hamming weight k , where n is the number of qubits and a computational basis state has Hamming weight k if exactly k of the bits take on value 1, e.g. $|D_2^4\rangle = \frac{1}{\sqrt{6}}(|1100\rangle + |1010\rangle + |1001\rangle + |0110\rangle + |0101\rangle + |0011\rangle)$. The combinatorial interpretation of a Dicke state is, for example, the set of all feasible solutions of a constraint optimization problem, such as Maximum k -Densest Subgraph, which asks for a subset of exactly k vertices of a given input graph with a maximum number of (induced) edges.

*Research presented in this article was supported by the Laboratory Directed Research and Development program of Los Alamos National Laboratory under project number 20200671DI. Report LA-UR-21-31138. Corresponding authors: saktar@nmsu.edu, baertschi@lanl.gov.

Table 1: Different preparation schemes for Dicke and related states. W States are Dicke States of Hamming weight 1, while Symmetric States are superpositions of Dicke States. They can thus be seen as a subset (superset, respectively) of Dicke States. Probabilistic state preparation uses a projective measurement of a n -qubit product state into a Hamming weight subspace. Quantum compression is more general and is used in reverse for state preparation. ε denotes the precision of arithmetic circuits.

This work improves circuits and constant factors from the work of Bärtschi and Eidenbenz [3].

| State Prep. | Reference | State Type | # CNOT Gates | Circuit Depth | # Ancillas |
|---------------|--------------------------------|------------------|--|--|------------------------------------|
| Probabilistic | Childs <i>et.al.</i> '00 [7,] | Dicke States | $\mathcal{O}(n \text{ poly log } n)$ | $\mathcal{O}(n \text{ poly log } n)$ | $\mathcal{O}(\log n)$ |
| Deterministic | Cruz <i>et.al.</i> '18 [10] | W States | $\mathcal{O}(n)$ | $\mathcal{O}(\log n)$ | – |
| | Kaye, Mosca '04 [25] | Symmetric States | $\mathcal{O}(n \text{ poly log } (n/\varepsilon))$ | $\mathcal{O}(n \text{ poly log } (n/\varepsilon))$ | $\mathcal{O}(\log(n/\varepsilon))$ |
| | Bärtschi, Eidenbenz '19 [3] | Dicke States | $\mathcal{O}(kn)$ | $\mathcal{O}(n)$ | – |
| | | Symmetric States | $\mathcal{O}(n^2)$ | $\mathcal{O}(n)$ | – |
| Uncompression | Bacon <i>et.al.</i> '04 [2] | Schur Transform | $\mathcal{O}(n \text{ poly log } (n/\varepsilon))$ | $\mathcal{O}(n \text{ poly log } (n/\varepsilon))$ | $\mathcal{O}(\log(n/\varepsilon))$ |
| | Plesch, Bužek '09 [33] | Symmetric States | $\mathcal{O}(n^2)$ | $\mathcal{O}(n^2)$ | – |

In this paper, we study how well Dicke states can be created on present-day Noisy Intermediate Scale Quantum (NISQ) devices, in particular several IBM Q devices. In Section 3, we propose a novel Divide-and-Conquer approach to designing Dicke state preparation circuits. We present circuits for Dicke states $|D_k^n\rangle$ for $1 \leq 2k \leq n \leq 6$ that are optimized towards minimum circuit depth and CNOT-gate counts. These circuits are our first main result. Compared to earlier work, we achieve reductions in CNOT counts of up to 30 percent; for instance our $|D_2^4\rangle$ circuit requires 10 CNOT gates and has a depth of 11 vs. previously best known values of 12 CNOT gates and a depth of 21 [26].

We test our circuits on two IBM Q backends (Sydney and Montreal) using several metrics and different compilation options that IBMs QISKIT environment offers. As our main measure to assess how close (noisy) these NISQ devices actually produce the (ideal pure) quantum state, we calculate the quantum fidelity of the state [22] through full state tomography. This requires the execution of 3^n different runs of our circuits which we measure in all possible Pauli bases, followed by a maximum-likelihood estimation of the density matrix representing the prepared mixed state [20], both of which are natively supported in QISKIT [37]. Each run needs to be repeated often enough in order to get sufficient statistics on the sampling frequency.

While we perform the computationally expensive full state tomography in all our experiments, we also explore alternatives. We study how well two simpler classical measures that each only require sufficient statistics on a single run upper bound the quantum fidelity. These two measures are the measured success probability (informally, how often do we sample a basis state with a Hamming weight k) and the Hellinger fidelity [17], an analog to quantum fidelity for classical probability distributions.

We test several different QISKIT compiler options that include giving an initial layout of logical to physical qubits, using noise adaptive transpilation (IBM's term for compilation [35]), or just a default transpilation, each combined with and without QISKIT's measurement error mitigation [36]. The details of our experimental setup as well as more formal definitions of our success measures are described in Section 4.

The contributions of this work can be summarized as follows with the details in Section 5:

1. Our novel Dicke state circuits lead to the best quantum fidelity results measured to date on IBM machines, e.g., a quantum fidelity for $|D_2^4\rangle$ of 0.87, which outperforms the previously measured best result of 0.53 [26].
2. As expected, quantum fidelity for these Dicke states decreases mostly with increasing circuit complexity; it appears to be a largely linear decrease with increasing CNOT counts. One particular notable exception to this rule is the use of noise-adaptive circuit compilation (which sometimes drastically increases CNOT counts).
3. Standard measurement error mitigation techniques increase the calculated quantum fidelity by an absolute value of around 0.1 with no clear dependence on circuit complexity. Relative improvements in achieved fidelity are seen for an increasing number of qubits n and a decreasing Hamming weight k (corresponding to circuits with many measurements but few gates).
4. The two IBM Q backends Sydney and Montreal exhibit quite different behaviors, with Montreal generally being much more stable, less susceptible to changes in compilation settings, and better achieved fidelity.
5. Our two alternative measures of Hellinger fidelity and measured success probability show a similar, albeit flatter linear dependence on CNOT count. Both measures upper bound the quantum fidelity with gaps growing larger with increasing circuit complexity.

Our results show clear technological progress in NISQ devices towards the ability to create entangled states, particularly when compared to experiments from one year ago. Parts of these improvements are due to our novel circuit design.

2 Related work

Due to their high entanglement, Dicke states [12] have been considered in fields such as quantum game theory [48], quantum networking [34], quantum metrology [40, 32], quantum error correction [29, 30] and quantum storage [31]. Their interpretation as superpositions of all feasible states in Hamming-weight constrained problems have also made them suitable candidates for initial states of adiabatic [7] and variational combinatorial algorithms [16, 41, 9, 6, 15, 14]. They have been implemented in various platforms such as trapped ions [18, 19, 23], atoms [39, 45, 38], photons [34, 42], superconducting qubits [43], and others [21, 44]. A Dicke State is defined as an equal superposition of all n -bit basis states x of Hamming weight $\text{wt}(x) = k$,

$$|D_k^n\rangle = \binom{n}{k}^{-\frac{1}{2}} \sum_{x \in \{0,1\}^n, \text{wt}(x)=k} |x\rangle. \quad (1)$$

Proposed state preparation *circuits* have first relied on arithmetic operations using ancilla registers [25, 2] until Plesch and Bužek [33] gave a quantum compression circuit for symmetric states using $\mathcal{O}(n^2)$ gates and depth but no ancillas, see Table 1. This circuit, used in reverse

Table 2: Comparing CNOT counts in our $|D_k^n\rangle$ preparation circuits versus previous approaches for $k = 1$ (Cruz *et.al.* 2018 [10]) and for $k = 2, 3$ (Mukherjee *et.al.* 2020 [26]). Our CNOT counts are attained on LNN architectures, with improved counts for Ladder architectures. $|D_{n-k}^n\rangle = X^{\otimes n} |D_k^n\rangle$ gives symmetric values for $k > n/2$.

| | # CNOTs (LNN) | | | | | # CNOTs (ladder) | | | | | prev # CNOTs | | | | |
|---------|---------------|---|----|----|----|------------------|---|---|----|----|--------------|---|----|----|----|
| | $n = 2$ | 3 | 4 | 5 | 6 | $n = 2$ | 3 | 4 | 5 | 6 | $n = 2$ | 3 | 4 | 5 | 6 |
| $k = 1$ | 1 | 3 | 5 | 7 | 9 | 1 | 3 | 5 | 7 | 9 | 1 | 3 | 5 | 7 | 9 |
| $k = 2$ | | | 10 | 17 | 24 | | | 7 | 14 | 21 | | | 12 | 20 | 28 |
| $k = 3$ | | | | | 32 | | | | | 23 | | | | | 33 |

with inverse operations, can be used to prepare Dicke states, because the permutation-invariant symmetric states are simply superpositions of Dicke states of different Hamming weight k .

An improved approach by Bärtschi and Eidenbenz [3] led to state preparation circuits for symmetric states with $\mathcal{O}(n^2)$ gates but linear $\mathcal{O}(n)$ depth even for Linear Nearest Neighbor (LNN) architectures. They also observed that by constricting the symmetric states' Hamming weights to $\leq k$, the number of gates can be decreased to $\mathcal{O}(nk) \subset \mathcal{O}(n^2)$. Mukherjee *et.al.* [26] later found that narrowing the Hamming weight constriction to exactly k , (*i.e.* Dicke States), additional gains in lower-order terms of $\mathcal{O}(k^2)$ can be made. Unfortunately, both of these gate reduction techniques result in either the need for much higher than LNN connectivity or the introduction of large constant factors in the gate count [3].

In this paper, we circumvent this problem to some extent by dividing a Dicke state preparation into two parts, where we first distribute the Hamming weight k over two contiguous blocks of $\lceil n/2 \rceil$ and $\lfloor n/2 \rfloor$ qubits each, before conquering each block with the mentioned LNN scheme. *Going forward, we restrict ourselves to Hamming weights $k \leq \lfloor n/2 \rfloor$, as a Dicke state $|D_{n-k}^n\rangle$ can easily be obtained by flipping all qubits (applying $X^{\otimes n}$) in the Dicke state $|D_k^n\rangle$.* Dividing the Hamming weight in general works best on Ladder architectures, with an increasing CNOT count on LNN connectivities. For the special case of Dicke states $|D_1^n\rangle$ with Hamming weight 1 (known as W states), this method retrieves the best-known CNOT counts of $2n - 3$, see Table 2.

Previous works [47, 1] have also included divide-and-conquer strategies for preparing arbitrary quantum states with reduced circuit depth. Recently, preparation circuits have been proposed for sparse quantum states [11, 24, 46] in terms of the number of non-zero state vector entries, requiring logarithmic depth but a quasi-linear number of ancillary qubits and gates. Dicke states can be treated as sparse quantum states for constant Hamming weight, but the number of non-zero entries in Dicke states scales exponentially as $\binom{n}{k}$ with increasing Hamming weight k . Hence, sparse state preparation circuits quickly become infeasible for Dicke states preparation.

Additionally, we note a probabilistic state preparation approach [7] that yields Dicke states with success probability $\binom{n}{k} (\frac{k}{n})^k (1 - \frac{k}{n})^{n-k}$ by preparing the symmetric n -qubit product state $(\sqrt{1 - k/n} |0\rangle + \sqrt{k/n} |1\rangle)^{\otimes n}$, followed by the addition [8] of the Hamming weight into an ancilla register with $\log n$ qubits and a projective measurement thereof. We use the first

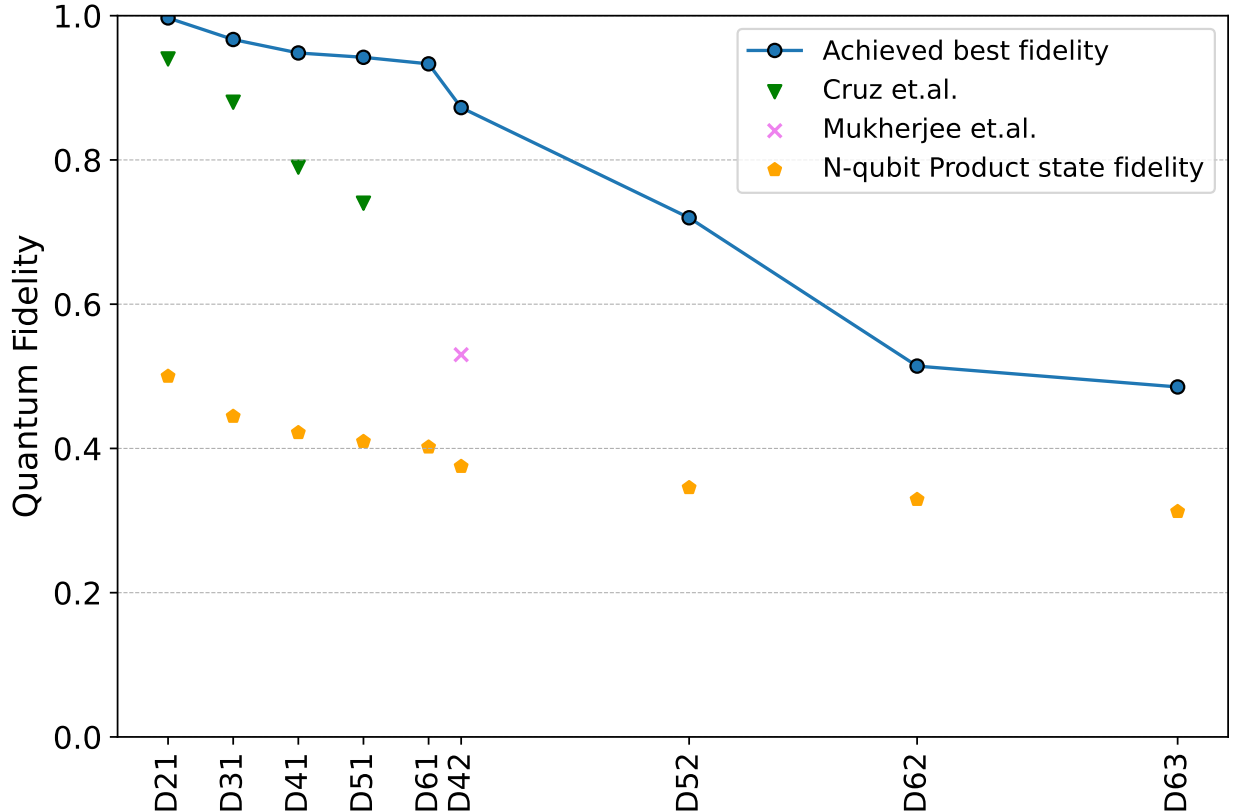


Figure 1: Comparison of our highest measured quantum fidelities with three benchmarks: measured fidelities for five W states $|D_1^n\rangle$ (Cruz *et.al.* 2018 [10]) and the Dicke state $|D_2^4\rangle$ (Mukherjee *et.al.* 2020 [26]), as well as the best possible fidelity among all n -qubit *product states*. Dicke states are distributed horizontally according to our CNOT counts.

part of this idea by using the fidelity between such a product state and the Dicke state $|D_k^n\rangle$ (corresponding to the success probability of the projective measurement) as an additional benchmark for our quantum fidelity results, see Figure 1. We additionally prove that no other pure n -qubit product state has higher fidelity / squared state overlap with the corresponding Dicke state.

3 Divide-and-Conquer Circuits

In this section, we give an overview of the techniques behind our Dicke state preparation circuits from Algorithm 1. They can best be described as a Divide-and-Conquer approach, where the “Conquer” part is based on improved versions of *Dicke state unitaries* [3] and the initial “Divide” part uses the new idea of distributing the Hamming weight across two contiguous blocks of qubits. We explain the implementation of Dicke state unitaries, distinguishing between big-endian notation (most significant bit – the “big end” – on the left of the bit string) and little-endian notation (reversed ordering) for their input encodings. We

Algorithm 1: Preparing Dicke State $|D_k^n\rangle$

Step-1: Divide the Hamming weight k

between two registers with $\lfloor n/2 \rfloor$ and $\lceil n/2 \rceil$ qubits.

/ On a Ladder architecture, this requires $\mathcal{O}(k)$ circuit depth & gate count.*

*On a LNN architecture, this requires $\mathcal{O}(k)$ circuit depth with $\mathcal{O}(k^2)$ gates. */*

/ We optimized the 'Divide' circuits specifically for LNN to account for the sparse connectivity of IBM devices, and describe the tuning of the circuits in Figures 4-6. */*

Step-2: Conquer the blocks

by implementing Dicke state unitaries on both registers.

/ Our implementation requires $\mathcal{O}(n)$ circuit depth and $\mathcal{O}(kn)$ gate count. */*

first briefly review Dicke state unitaries $U_{n,k}$ which denote any unitary satisfying

$$\forall k' \leq k: U_{n,k} |0^{n-k'} 1^{k'}\rangle = |D_{k'}^n\rangle. \quad (2)$$

That is, $U_{n,k}$ takes as possible input a zero-padded unary encoding of any Hamming weight $k' \leq k$ to prepare the Dicke state $|D_{k'}^n\rangle$.

Previous approaches to prepare $|D_k^n\rangle$ simply fed the input $|0^{n-k} 1^k\rangle$ to $U_{n,k}$ [10, 3]. In this paper, we present a new approach in which we first divide the Hamming weight into all possible combinations of $k_1 + k_2 = k$ across two blocks of $n_1 + n_2 = n$ qubits, followed by two parallel Dicke state unitaries U_{n_1,k_1} , U_{n_2,k_2} on these blocks. By doing so, we must give the correct weights to the corresponding unary encodings $|0^{n_1-k_1} 1^{k_1}\rangle |0^{n_2-k_2} 1^{k_2}\rangle$. Since there are $\binom{n_1}{k_1} \binom{n_2}{k_2}$ computational basis states with Hamming weight k_1 in the n_1 -bit-prefix and Hamming weight k_2 in the n_2 -bit-suffix, the ‘‘Divide’’ part consists of preparing the state

$$\frac{1}{\sqrt{\binom{n}{k}}} \sum_{k_1+k_2=k} \sqrt{\binom{n_1}{k_1} \binom{n_2}{k_2}} |0^{n_1-k_1} 1^{k_1}\rangle |0^{n_2-k_2} 1^{k_2}\rangle. \quad (3)$$

We next discuss Dicke state unitaries – the ‘‘Conquer’’ part of our circuits – and our improved implementations thereof in detail, before giving the ‘‘Divide’’ part for both Ladder and LNN architectures.

3.1 ‘‘Conquer’’: Dicke State Unitaries

Dicke state unitaries $U_{n,k}$ [3, (2)] implement the induction

$$|D_{k'}^{n'}\rangle = \sqrt{\frac{k'}{n'}} |D_{k'-1}^{n'-1}\rangle \otimes |1\rangle + \sqrt{\frac{n'-k'}{n'}} |D_{k'}^{n'-1}\rangle \otimes |0\rangle$$

for all $n' \leq n$, $k' \leq \min\{k, n'\}$. Given that $U_{n,k}$ gets as input $|0^{n-k'} 1^{k'}\rangle$, it is enough to implement for all $k' \leq k$ the gate $|0^{n-k'} 1^{k'}\rangle \mapsto \sqrt{\frac{k'}{n}} |0^{n-k'} 1^{k'}\rangle + \sqrt{\frac{n-k'}{n}} |0^{n-k'-1} 1^{k'} 0\rangle$ followed by a recursive call to the smaller unitary $U_{n-1,k}$, see Figures 2, 3.

For $U_{n,1}$ and $k' = 0, 1$, this involves CNOTs and a controlled $R_y(2 \cos^{-1} \sqrt{\frac{1}{n}})$ -rotation, which we compile down to two single-qubit $R_y(\pm \frac{1}{2} \cdot 2 \cos^{-1} \sqrt{\frac{n-1}{n}})$ rotations and two CNOTs. This places $U_{n-1,1}$ on the lower $n - 1$ wires, see Figure 3, and thus can be implemented even on LNN architectures.

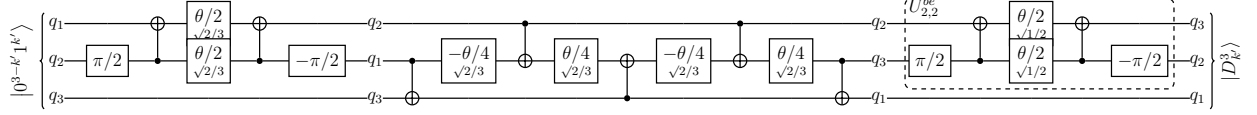


Figure 2: Implementation of the big-endian Dicke State Unitary $U_{3,3}^{be} = U_{3,2}^{be}$ which takes as input $|0^{3-k'} 1^{k'}\rangle$ for any k' to prepare $|D_{k'}^3\rangle$. A small-endian Dicke State Unitary $U_{3,3}^{le}$ has the wire order reversed and accepts inputs $|1^{k'} 0^{3-k'}\rangle$ instead.

The circuit incorporates SWAPs into the actions on the three logical qubits: $|001\rangle \mapsto \sqrt{\frac{1}{3}}|001\rangle + \sqrt{\frac{2}{3}}|010\rangle$ and $|011\rangle \mapsto \sqrt{\frac{2}{3}}|011\rangle + \sqrt{\frac{1}{3}}|110\rangle$, as well as $|01.\rangle \mapsto \sqrt{\frac{1}{2}}|01.\rangle + \sqrt{\frac{1}{2}}|10.\rangle$ in the unitary $U_{2,2}^{be}$. This changes the ordering of the logical qubits throughout the circuit as shown, where the final order does not matter due to the symmetry of the final state $|D_{k'}^3\rangle$.

For $U_{n,k}$ with $k' > 1$, we have longer blocks of excitations in the state $|0^{n-k'} 1^{k'-1} 1^1\rangle$ which has to be mapped to $\sqrt{\frac{k'}{n}}|0^{n-k'} 1^{k'-1} 1^1\rangle + \sqrt{\frac{n-k'}{n}}|0^{n-k'} -1 1^1 1^{k'-1} 0\rangle$. Still, only three qubits are necessary for this gate, the two qubits changing 0/1-values and the leading 1 as a control. The gate can be compiled to CNOTs and a doubly-controlled $R_y(2 \cos^{-1} \sqrt{\frac{k'}{n}})$ -rotation [3]. In order to implement the gate on three contiguous blocks of qubits, we incorporate SWAPs which move the lowest-endian qubit from top to bottom, see Figure 2. This keeps the CNOT count for gates with $k' = 1$ intact, while for $k' > 1$ we get an implementation with 5 CNOTs and 4 $R_y(\pm \frac{1}{4} \cdot 2 \cos^{-1} \sqrt{\frac{k'}{n}})$ -rotations. Finally, we recurse from $U_{n,k}$ to $U_{n-1,k}$ (where in case $k = n$, we use $U_{n,n} = U_{n,n-1}$ to get $U_{n-1,n-1}$). The detailed shifting-down procedure for the lowest-endian qubit places $U_{n-1,k}$ on the upper $n - 1$ wires.

Finally, we note that our descriptions assumed big-endian inputs $|0^{n-k'} 1^{k'}\rangle$ and thus we further specify the given Dicke state unitaries by $U_{n,k}^{be}$. A little-endian version $U_{n,k}^{le}$ accepting little-endian inputs $|1^{k'} 0^{n-k'}\rangle$ is achieved by simply reversing the wire order. The ‘‘Divide’’ procedure discussed next will result in an application of both types of Dicke state unitaries, namely $U_{\lfloor n/2 \rfloor, k}^{be}$ and $U_{\lfloor n/2 \rfloor, k}^{le}$.

3.2 ‘‘Divide’’ for Ladder Topologies

In hardware with ladder architectures, we have two rows of qubits which are provided with 2-qubit gates towards their horizontal nearest neighbors, as well as with their direct neighbor below, respectively above. Such topologies can be found, for example, as subgraphs of Google’s sycamore processor and until recently, among IBM Q’s devices. The ‘‘Divide’’ technique in the following can also be applied (with constant overhead) to sparser connectivities such as IBM Q’s heavy-hex lattices or serve as an inspiration for an adaption to LNN architectures discussed in the next subsection.

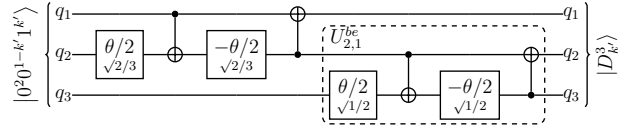


Figure 3: Implementation of the Dicke State Unitary $U_{3,1}^{be}$, which takes as input the padded big-endian unary encoding of $k' \leq 1$, (i.e., $|0^2 0^{1-k'} 1^{k'}\rangle$) to create the Dicke State $|D_{k'}^3\rangle$. Labeled gates are R_y -rotations, where $\theta_{\sqrt{x/y}} = 2 \cos^{-1} \sqrt{\frac{x}{y}}$. The first half of the circuit implements $|001\rangle \mapsto \sqrt{\frac{1}{3}}|001\rangle + \sqrt{\frac{2}{3}}|010\rangle$, the second half the recursively used unitary $U_{2,1}^{be}$.

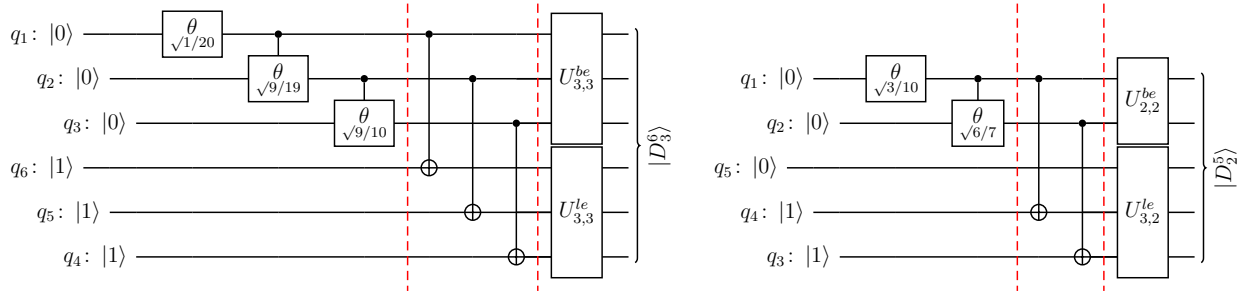


Figure 4: Preparations of Dicke States on ladder topologies with a divide-and-conquer approach: The Hamming weight k is divided between an upper big-endian row of $n_1 = \lfloor n/2 \rfloor$ qubits and a lower, little-endian row of $n_2 = \lceil n/2 \rceil$ qubits. The resulting superposed entangled row input weights are conquered with the unitaries $U_{n_1,k}^{be}$ and $U_{n_2,k}^{le}$, respectively. (LEFT) First we construct the weighted big-endian superposition $\sqrt{\frac{1}{20}}(\sqrt{1}|000\rangle + \sqrt{9}|001\rangle + \sqrt{9}|011\rangle + \sqrt{1}|111\rangle)$ in the upper row. Note that the numerators 1, 9, 9 and the suffix sums 20, 19, 10 appear as terms in the angle arguments. Next we subtract these weights from the little-endian Hamming weight $k = 3$ in the lower row. Finally we use Dicke State unitaries on both rows to construct $|D_3^6\rangle$. (RIGHT) Same approach for $|D_2^5\rangle$, where we first construct $\sqrt{\frac{1}{10}}(\sqrt{3}|00\rangle + \sqrt{6}|01\rangle + \sqrt{1}|11\rangle)$ in the upper row and subtract from Hamming weight $k = 2$ in the lower row.

Recall that we restrict ourselves to Hamming weight values $k \leq n/2$ due to the symmetry $|D_k^n\rangle = X^\otimes |D_k^n\rangle$. We divide our n qubits into $n_1 = \lfloor n/2 \rfloor$ qubits q_1, \dots, q_{n_1} on the upper row and $n_2 = \lceil n/2 \rceil$ qubits q_n, \dots, q_{n_1+1} (in this order) on the lower row, such that qubit q_i , $i \leq n_1$ is vertically connected to qubit q_{2n_1-i+1} , see Figure 4.

To get the desired state from Equation (3), we first prepare

$$\frac{1}{\sqrt{\binom{n}{k}}} \sum_{k_1+k_2=k} \sqrt{\binom{n_1}{k_1} \binom{n_2}{k_2}} |0^{n_1-k_1} 1^{k_1}\rangle |0^{n_2-k} 1^k\rangle.$$

Let $x_i = \binom{n_1}{i} \binom{n_2}{k-i}$ denote the number of bitstrings with Hamming weight i among the first half of n_1 digits and Hamming weight $k - i$ among the second half of $n_2 = n - n_1$ digits. Of the sequence x_0, \dots, x_k , let $s_i = x_i + \dots + x_k$ denote the suffix sums of the x_i -values. Then, we can construct the superposition $\sum_{k_1+k_2=k} \sqrt{\binom{n_1}{k_1} \binom{n_2}{k_2}} |0^{n_1-k_1}\rangle$ (modulo proper normalization) one term at a time with controlled $R_y(2 \cos^{-1} \sqrt{\frac{x_i}{s_i}})$ -rotations *up until* $i = k - 1$; consecutively rotating qubits one-by-one controlled on the value of previous, smaller-endian qubits, see Figure 4. The compilation of a CR_y -gate into single-qubit and CNOT gates usually takes 2 CNOTs, however for a classical 0-or-1 target, it can be done with 1 CNOT only (with compilation based on knowledge of the classical value).

We can then subtract (in superposition) the Hamming weight k_1 encoded in big-endian unary in the first half of n_1 qubits from the $|0^{n_2-k} 1^k\rangle$ unary encoding of k in the second half of n_2 qubits. This can be done with 1 CNOT for each pair (q_i, q_{2n_1-i+1}) . Taking also into account the number of CNOTs of a big-endian unitary $U_{n_1,k}^{be}$ on the upper n_1 qubits and a little-endian unitary $U_{n_2,k}^{le}$ on the lower, reversely ordered n_2 qubits, we get the CNOT counts for Ladder architectures in Table 2.

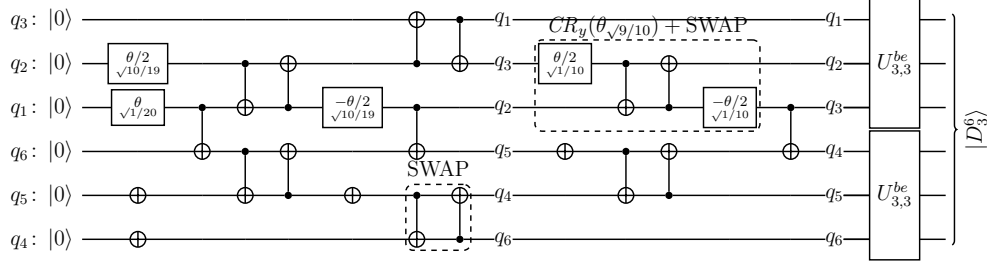


Figure 5: Implementation of Dicke state $|D_3^6\rangle$ on LNN starting from a reverse ordering of the qubit blocks (q_1, q_2, q_3) and (q_4, q_5, q_6) : We start with neighboring qubits q_1, q_6 , implement their interaction and then swap them to the far ends of the circuit. While doing so, we use the fact that controlled- R_y s and SWAPs target qubits in a classical state, which reduces implementations of SWAP and $CR_y + \text{SWAP}$ interactions to two CNOTs each.

For the “Divide” part we get a CNOT count of 15 and a CNOT depth of 8, while for the “Conquer” part in the big-endian unitaries $U_{3,3}^{be}$ we have 9 CNOTs. Overall we get a CNOT count of 33 and a CNOT depth of 17.

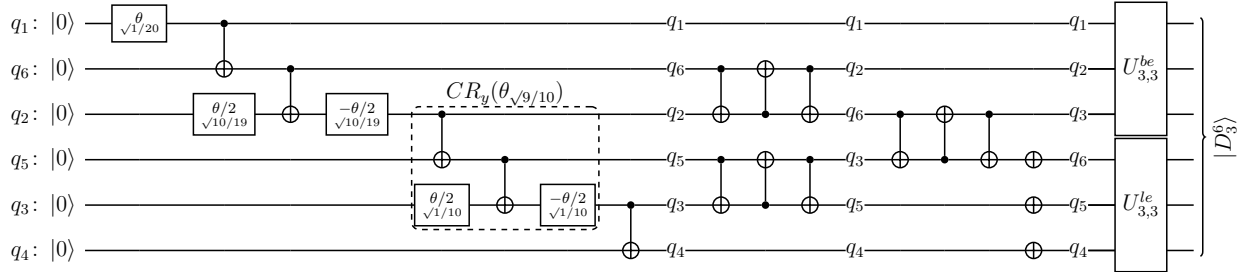


Figure 6: Implementation of Dicke state $|D_3^6\rangle$ on LNN starting from an interleaved ordering of the qubit blocks (q_1, q_2, q_3) and (q_4, q_5, q_6) : We use the interjacently placed qubits q_6, q_5, q_4 while preparing the qubits q_1, q_2, q_3 . While doing so, their assignment is flipped compared to the supposed superposition, hence we apply X -gates in the last step of the “Divide” part. CR_y gates still target qubits in a classical state, hence they can be implemented with 1 CNOT each. Un-interleaving now needs SWAPs to be decomposed into 3 CNOTs each. Furthermore, the circuit parallelizes less than the method given in Figure 5.

For the “Divide” part we get a CNOT count of 14 and a CNOT depth of 11, while for the “Conquer” part in the big/little-endian unitaries $U_{3,3}^{be}$, $U_{3,3}^{le}$ we have 9 CNOTs. Overall we get a CNOT count of 32 and a CNOT depth of 20.

3.3 “Divide-and-Conquer” for LNN Topologies

In our experiments, we are restricted to way sparser architectures. Hence, we additionally fine-tune the “Divide” techniques for Ladder architectures to Linear Nearest Neighbor architectures. We utilized two methods for this:

In the simplest way, we start from the Ladder architecture of Figure 4 and remove vertical connectivities except for (q_1, q_{2n_1}) . We then exchange for each qubit q_i , $i < n_1$ the order of the CR_y and the subtraction CNOT it controls. When adding SWAPs and combining each CR_y gate with one of the SWAP gates, we get the LNN circuit in Figure 5. Note that, in

this case, the SWAPs as well as the combination of CR_y and SWAP gates compile to two CNOTs only, since at the moment of applying the gates, their target is still in a classical state.

An additional option is given in Figure 6. Here the circuits starts with the qubits (q_1, \dots, q_{n_1}) and (q_n, \dots, q_{n_1+1}) interleaved. This approach works best for the Dicke state $|D_2^6\rangle$ and also decreased the CNOT count for the Dicke state $|D_3^6\rangle$ while simultaneously increasing the CNOT depth. Hence we used this approach in experiments for exclusively for $|D_2^6\rangle$ and both approaches for $|D_3^6\rangle$.

For $k = 1$ the first approach retrieves the circuits of previous W-state experiments [10]. Interactive drag-and-drop implementations of our circuits in the Quirk simulator [13] are behind the following links: [|D₁²⟩](#), [|D₁³⟩](#), [|D₁⁴⟩](#), [|D₂⁴⟩](#), [|D₁⁵⟩](#), [|D₂⁵⟩](#), [|D₁⁶⟩](#), [|D₂⁶⟩ \(interleaved\)](#), [|D₃⁶⟩](#), [|D₃⁶⟩ \(interleaved\)](#).

4 Methods

In this section, we discuss our experimental setup, the evaluated metrics (quantum state fidelity, Hellinger fidelity, and measured success probability), as well as relations between those and existing benchmarks.

4.1 Definitions

Informally, our goal is to measure how well our circuits prepare the Dicke states $|D_k^n\rangle$ for $n \leq 6$, $k \leq n/2$ on IBM Q devices Sydney and Montreal. To make this precise, we first introduce some notation. On one hand, on an ideal quantum device, our circuits would prepare the pure quantum state $\delta := |D_k^n\rangle\langle D_k^n|$. When measured in the computational basis, the probability q_i to get basis state $|i\rangle$ is

$$q_i = \text{tr}(|i\rangle\langle i| \delta) = \langle i | D_k^n \rangle \langle D_k^n | i \rangle = \begin{cases} \frac{1}{\binom{n}{k}} & \text{if } \text{wt}(i) = k, \\ 0 & \text{otherwise.} \end{cases} \quad (4)$$

On the other hand, due to noise on current NISQ devices, the circuits prepare a noisy mixed state [28], denoted with the density matrix ρ , a positive semi-definite Hermitian matrix. A computational basis measurement gives basis state $|i\rangle$ with probability $p_i := \text{tr}(|i\rangle\langle i| \rho) = \langle i | \rho | i \rangle = \rho_{ii}$. As we can neither directly observe the mixed state ρ nor the probabilities $(p_i)_i$, we fit the results of quantum state tomography circuits with a maximum-likelihood estimation [20], while we use relative frequencies of sampling $|i\rangle$ to estimate the probability p_i . All of this is natively supported in QISKIT [37].

As an example, we show density matrices $\delta = |D_2^4\rangle\langle D_2^4|$ and ρ as state city plots in Figure 7, with two versions of the experimentally derived ρ : one that we get from the state tomography circuit results, and one which we get from the results combined with measurement error mitigation, discussed in Subsection 4.3 and in more detail in 5.2.

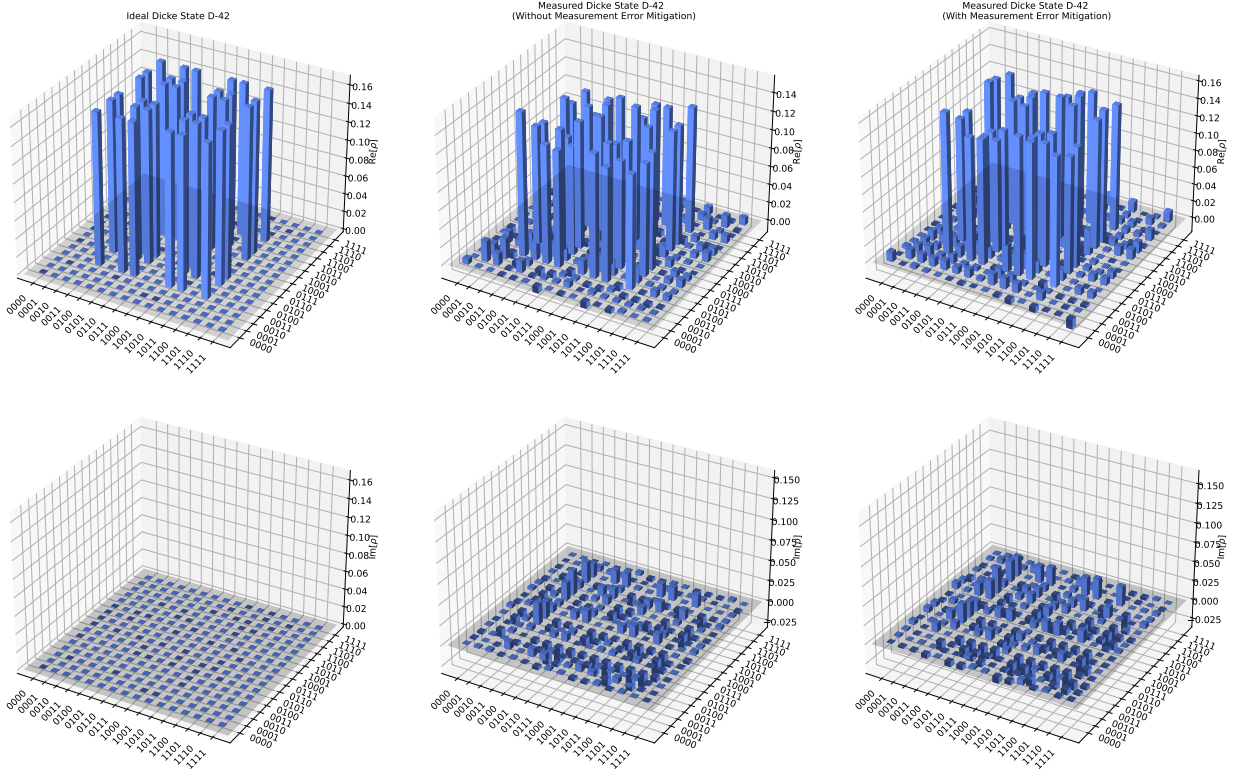


Figure 7: State city plots of (LEFT) pure Dicke State $|D_2^4\rangle\langle D_2^4|$, (MIDDLE) measured state ρ , (RIGHT) error-mitigated ρ . In each column, the (TOP) plot shows the real value of the corresponding density matrix entry ρ_{ij} and the (BOTTOM) plot the imaginary part. The measured states were prepared on IBM Q Montreal using state tomography circuits with an initial layout provided transpilation, with and without the use of measurement error mitigation.

4.1.1 Quantum Fidelity

Quantum state fidelity is a quantitative measure on the closeness of two quantum states. In our context, it measures how close the output state ρ of a Dicke state preparation circuit is to the ideal expected state $|D_k^n\rangle$. Thus the fidelity signifies the probability that ρ passes the yes/no test of being the pure $|D_k^n\rangle$ (with the test being the measurement of the observable $\delta = |D_k^n\rangle\langle D_k^n|$) [22].

More generally, the fidelity between δ and ρ can range from 0 to 1 and is defined as¹

$$F(\delta, \rho) = \left[\text{tr} \left(\sqrt{\sqrt{\delta} \rho \sqrt{\delta}} \right) \right]^2, \quad (5)$$

where $\sqrt{\rho}$ denotes the unique positive semi-definite square root of ρ such that $\sqrt{\rho} \sqrt{\rho} = \rho$. Since δ in our case is pure and thus $\sqrt{\delta} = \delta$, Equation 5 reduces to

$$F(|D_k^n\rangle, \rho) = \langle D_k^n | \rho | D_k^n \rangle. \quad (6)$$

¹We note that some authors [28] use the non-squared trace as an alternative definition for fidelity, $F'(\delta, \rho) = \text{tr} \sqrt{\sqrt{\delta} \rho \sqrt{\delta}}$.

Finally, if ρ were a pure state as well, $\rho = |\psi\rangle\langle\psi|$, the fidelity would reduce to the squared state overlap

$$F(|D_k^n\rangle, \psi) = |\langle D_k^n | \psi \rangle|^2. \quad (7)$$

To determine the density matrix ρ describing the mixed state prepared by our Dicke state circuits on IBM Q devices, we run full state tomography with 3^n different circuits, each sampling the prepared state in a particular Pauli basis.

4.1.2 Hellinger Fidelity

In the case of classical probabilities (where density matrices reduce to diagonal matrices with $\delta_{ii} = q_i$, $\rho_{ii} = p_i$), the quantum fidelity (5) reduces to an analogous measure for the similarity between two probability distributions $p = (p_i)_i$, $q = (q_i)_i$ called Hellinger fidelity

$$H(q, p) = \left[\sum_{i=1}^n \sqrt{p_i \cdot q_i} \right]^2. \quad (8)$$

The Hellinger fidelity is related to maybe better known measures Hellinger distance HD = $\frac{1}{\sqrt{2}}\sqrt{\sum(\sqrt{p_i} - \sqrt{q_i})^2}$ [17] and Bhattacharya coefficient BC = $\sum \sqrt{p_i \cdot q_i}$ [5] through HD = $BC^2 = (1-HD^2)^2$.

The Hellinger fidelity between the ideal Dicke state probability distribution q_i from Equation 4 and the measurement probabilities $p_i = \rho_{ii}$ for Dicke states prepared on IBM Q only depends on the diagonal elements of the state's density matrix ρ , thus ignoring information on coherence between different basis states. On the plus side, this circumvents the high number of tomography circuits, as p_i can be estimated from the relative frequency of samples $|i\rangle$ we get from measuring the Dicke state preparation circuit in the computational basis.

4.1.3 Measured Success Probability

An even more simplistic measure has been used in the literature [26], which is to simply estimate the probability that a measurement in the computational basis yields a state $|i\rangle$ with Hamming weight $\text{wt}(i) = k$. We call this the measurement success probability:

$$M_k(p) = \sum_{\text{wt}(i)=k} p_i. \quad (9)$$

The measurement success probability not only drops the evaluation of coherence, but also does not discriminate between a uniform distribution over Hamming weight k states and skewed distributions with the same success probability. We now explore the relation between the three measures from Equations (6), (8) and (9) and existing benchmarks.

4.2 Relationship of measures, benchmarks

As we have seen, the measures quantum fidelity F , Hellinger fidelity H and measurement success probability M_k intuitively are increasingly less strict. This is also true mathematically,

i.e. we show the relation $F \leq H \leq M_k$:

$$\begin{aligned}
F(|D_k^n\rangle, \rho) &= \langle D_k^n | \rho | D_k^n \rangle = \langle D_k^n | Id \sqrt{\rho}^\dagger \sqrt{\rho} Id | D_k^n \rangle \\
&= \sum_{i=1}^n \sum_{j=1}^n \langle D_k^n | i \rangle \langle i | \sqrt{\rho}^\dagger \sqrt{\rho} | j \rangle \langle j | D_k^n \rangle \\
&\stackrel{CS}{\leq} \sum_{i=1}^n \sum_{j=1}^n \underbrace{\langle D_k^n | i \rangle}_{\sqrt{q_i}} \underbrace{\langle i | \rho | i \rangle}_{\sqrt{p_i}} \underbrace{\langle j | \rho | j \rangle}_{\sqrt{p_j}} \underbrace{\langle j | D_k^n \rangle}_{\sqrt{q_j}} \\
&= \left(\sum_{i=1}^n \sqrt{q_i p_i} \right)^2 = H(p, q) \stackrel{(4)}{=} \left(\sum_{\text{wt}(i)=k} \sqrt{q_i} \sqrt{p_i} \right)^2 \\
&\stackrel{CS}{\leq} \left(\sum_{\text{wt}(i)=k} q_i \right) \left(\sum_{\text{wt}(i)=k} p_i \right) \stackrel{(4)}{=} M_k(p),
\end{aligned}$$

where we used the Cauchy-Schwarz inequality (CS) and the q_i definition (4) twice each. \square

We will be interested in how well the classical measures Hellinger fidelity and measurement success probability *upper bound* the classical fidelity. Note that because ρ and p_i are only estimated through a maximum-likelihood fitter and relative frequencies of samples, respectively, there is a small chance for statistical fluctuations violating the inequalities.

In lieu of lower bounds, we turn instead to existing benchmarks for quantum fidelities with Dicke states (see Figure 1):

- quantum fidelities ranging from ~ 0.95 to ~ 0.75 [10] for W state preparation of $|D_1^2\rangle$, $|D_1^3\rangle$, $|D_1^4\rangle$, $|D_1^5\rangle$,
- quantum fidelity of 0.53 [26] for the $|D_2^4\rangle$ preparation,
- squared state overlaps (7) ranging from 0.5 to 0.3125 for product states $(\sqrt{1-k/n}|0\rangle + \sqrt{k/n}|1\rangle)^{\otimes n}$.

The latter is actually the state with highest quantum fidelity with $|D_k^n\rangle$ among all n -qubit product states. We will prove this formally, as it is not clear a priori: based on the symmetry of Dicke states, we know that any symmetric permutation of qubits in a product state can not change its squared state overlap with the Dicke state, however this does not imply directly that the best possible product state itself has to be symmetric. Let $|\psi\rangle = \bigotimes_{i=1}^n (a_i |0\rangle + b_i |1\rangle)$ be any n -qubit product state, where $|a_i|^2 + |b_i|^2 = 1$. We are interested in all terms of the state vector which have Hamming weight k , i.e. whose amplitudes consist of $n-k$ a s and k b s.

Then its quantum fidelity with $|D_k^n\rangle$ satisfies

$$\begin{aligned}
|\langle D_k^n | \psi \rangle|^2 &= \left| \frac{1}{\sqrt{\binom{n}{k}}} a_{i_1} \cdots a_{i_n} \sum_{1 \leq i_1 \leq \dots \leq i_k \leq n} \frac{b_{i_1}}{a_{i_1}} \cdots \frac{b_{i_k}}{a_{i_k}} \right|^2 \\
&\stackrel{CS}{\leq} \frac{1}{\binom{n}{k}} \left(\sum_{1 \leq i_1 \leq \dots \leq i_{n-k} \leq n} |a_{i_1}|^2 \cdots |a_{i_{n-k}}|^2 \right) \left(\sum_{1 \leq i_1 \leq \dots \leq i_k \leq n} |b_{i_1}|^2 \cdots |b_{i_k}|^2 \right) \\
&= \frac{\binom{n}{k}^2}{\binom{n}{k}} \left(\frac{\sum |a_{i_1}|^2 \cdots |a_{i_{n-k}}|^2}{\binom{n}{n-k}} \right) \left(\frac{\sum |b_{i_1}|^2 \cdots |b_{i_k}|^2}{\binom{n}{k}} \right) \\
&\stackrel{M}{\leq} \binom{n}{k} \left(\frac{\sum_{i=1}^n |a_i|^2}{n} \right)^{n-k} \left(\frac{\sum_{i=1}^n |b_i|^2}{n} \right)^k \\
&= \frac{\binom{n}{k}}{n^n k^{n-k} (n-k)^k} \left(k \sum |a_i|^2 \right)^{n-k} \left((n-k) \sum |b_i|^2 \right)^k \\
&\stackrel{GA}{\leq} \frac{\binom{n}{k}}{n^n k^{n-k} (n-k)^k} \left(\frac{(n-k)k \sum |a_i|^2 + k(n-k) \sum |b_i|^2}{n} \right)^n \\
&= \frac{\binom{n}{k} k^n (n-k)^n}{n^n k^{n-k} (n-k)^k} = \binom{n}{k} \left(\frac{k}{n} \right)^k \left(\frac{n-k}{n} \right)^{n-k},
\end{aligned}$$

using the Cauchy-Schwarz inequality (CS), the Maclaurin inequality for elementary symmetric polynomials (M) and the Geometric & Arithmetic Mean inequality (GA). In the inequalities, equality holds for Maclaurin if all $|a_i|^2$ are equal (and all $|b_i|^2$ are equal, respectively), for the Geometric & Arithmetic Mean if $(n-k) \sum |b_i|^2 = k \sum |a_i|^2$ and for Cauchy-Schwarz if the fractions $\frac{b_{i_1} \cdots b_{i_k}}{a_{i_1} \cdots a_{i_k}}$ have the same value for all index choices i_1, \dots, i_k . Equality along the whole chain thus holds if for all i we have $a_i = \sqrt{1 - k/n}$ and $b_i = \sqrt{k/n}$. \square

4.3 Experimental Setup

4.3.1 Measurement Error Mitigation:

Noise in gate-level quantum computers generates measurement results that are far away from the results expected from an ideal quantum computer. Unusual behavior of physical quantum gates and relaxation of quantum energy over time are considered the primary source of noise which represents a massive challenge in quantum computing. There is another form of noise that occurs during the final measurement step that affects the perfect output state and outputs randomly perturbed noisy state. It is possible to understand the effect of those measurement errors by first generating circuits for all possible 2^n basis states and measuring them on a real quantum system to find the probability of each states. Theoretically these perfect basis states becomes noisy before returning to the user as output i.e. $Output_{actual} = M_{noise} * Output_{ideal}$. If we can compute the matrix that when multiplied with the ideal state generates the measured state, it is possible to get the mitigated output. From linear algebra, the inverse of M_{noise} can be applied to mitigate the measurement errors from the $Output_{actual}$ state i.e. $Output_{mitigated} = M_{noise}^{-1} * Output_{actual}$ [36].

4.3.2 Transpilation

We construct circuits for Dicke States $|D_k^n\rangle$ where $n = 2, 3, 4, 5, 6$ and $k = 1, 2, 3$ using the divide and conquer approach described in Section 3. IBM QISKIT compiler (version: 0.26.2) is used to compile the logical circuits onto the specified hardware using the native gate set. As pre and post compiled circuits remain in the same language and both are equivalent in terms of unitary representation, the Qiskit compiler is termed a ‘transpiler’ while the compilation is termed as ‘transpilation’ [35]. QISKIT offers different transpilation & optimization options that generate custom transpiled circuits. For this experiment, we set the QISKIT optimization level to 3 and use three different transpilation options: i) **Default**: We only use the default options. ii) **Initial Layout Provided**: We provide a subgraph of the required number of qubits as the initial layout where we choose the qubits focusing on LNN connectivity & gate error rate. iii) **Noise Adaptive**: We set *layout_method* argument as *noise_adaptive* and depend on QISKIT to select qubits. In the noise adaptive mapping, the qubits are selected using the specific machine topology and daily calibration data from IBM. It avoids qubits with high error rates and low coherence times to enable maximum reliability for CNOTs and reduce qubit movements [27].

4.3.3 Evaluation

To verify the circuits, we compute the quantum fidelity to measure the closeness of the prepared state ρ to the Dicke state $|D_k^n\rangle$. To calculate ρ , we first generate state tomography circuits in each measurement combination of the Pauli X, Y, and Z bases for n -qubits that give a total of 3^n measurement circuits. We run the tomography circuits in IBM Q systems and calculate fidelity between pure output state and tomography circuit measurement. For this experiment, we selected IBM Q Sydney and IBM Q Montreal quantum systems from the IBM Quantum Experience cloud service. IBM Q Sydney and IBM Q Montreal have the same elongated hexagon topology on their 27 qubits. The quantum volume of IBM Q Sydney is 32 and the quantum volume of IBM Q Montreal is 128. The average CNOT gate error in IBM Q Sydney & IBM Q Montreal is 0.0114 and 0.1522 where the average readout error is 0.05078 and 0.02028, respectively.

We apply measurement calibration to mitigate noise in the final measurement steps of the tomography circuits. We use the QISKIT ignis package to mitigate the noise by first creating a measurement filter object, then applying the filter to the actual output state. Then we compute fidelity again between the ideal state and error mitigated output state to compare with the previous fidelity.

We also compare quantum fidelity with Hellinger fidelity and measured success probability for different transpilation options. For each experiment, we run all 3^n tomography circuits using ‘*qiskit.execute*’ where all the circuits are executed together, alternatively also using ‘*IBMQJobManager.run*’ where we split the circuits into multiple jobs and set to execute a fixed number of circuits in a job.

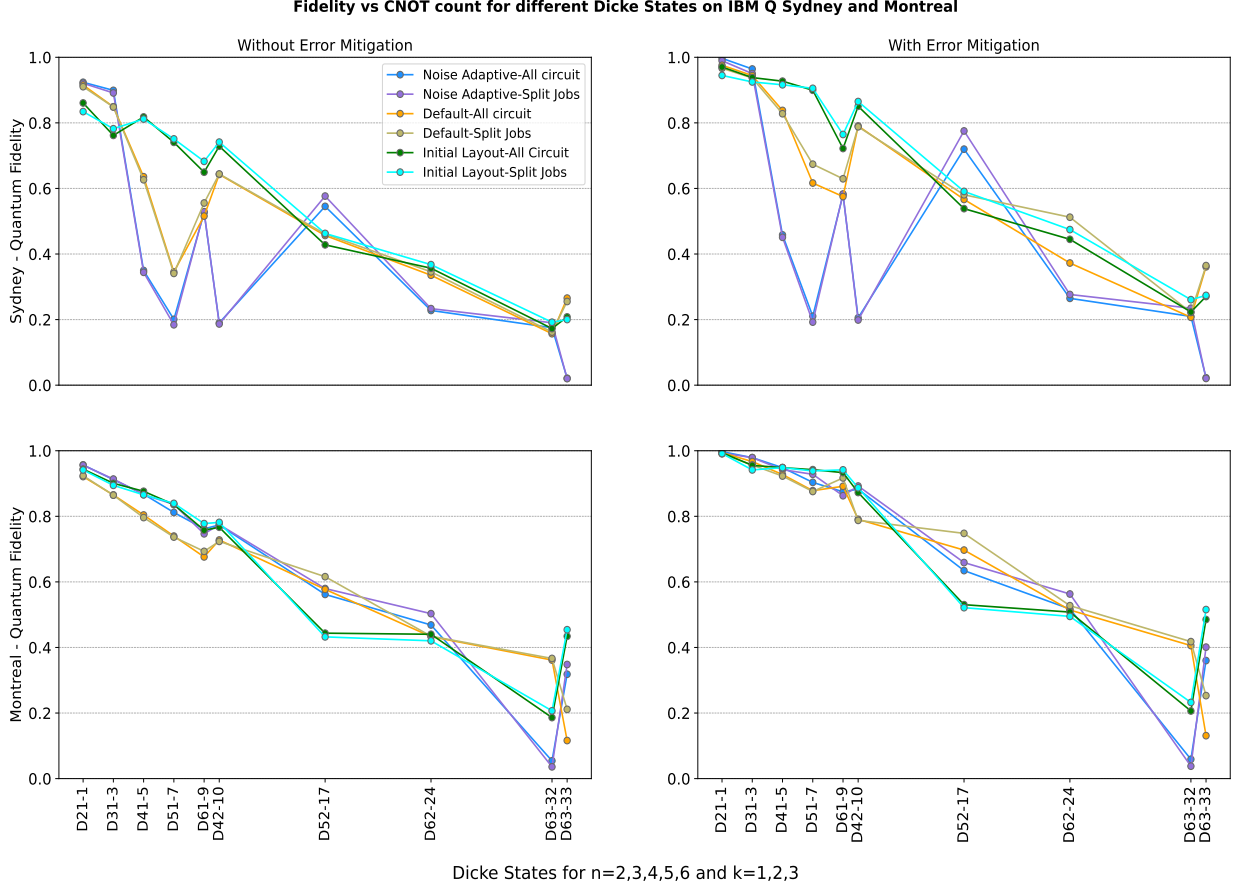


Figure 8: Measured fidelity of Dicke States for IBM Q Sydney system without error mitigation (top left) & with error mitigation (top right) and IBM Q Montreal system without error mitigation (bottom left) & with error mitigation (bottom right) using different transpilation method of QISKIT. We varied default, noise adaptive and initial layout provided transpilation of QISKIT with optimization level 3. Additionally we applied error mitigation techniques of QISKIT to reduce measurement noise from the output.

5 Results

We explain experimental results on IBM Q Sydney and Montreal systems for the different Dicke States using the transpilation options described in Subsection 4.3. We denote the Dicke State circuits as $Dnk-r$ where $n = \{2, 3, 4, 5, 6\}$ represents the number of qubits, $k = \{2, 3, 4, 5, 6\}$ represents the Hamming weight, and r denotes the number of CNOT gates in the circuit. All in all, the Dicke states $|D_2^1\rangle, |D_3^1\rangle, |D_4^1\rangle, |D_5^1\rangle, |D_6^1\rangle, |D_4^2\rangle, |D_5^2\rangle, |D_6^2\rangle$ and $|D_6^3\rangle$ are prepared by circuits D21 - 1, D31 - 2, D41 - 5, D51 - 7, D61 - 9, D42 - 10, D52 - 17, D62 - 24, D63 - 32, D63 - 33. The experiments using `qiskit.execute` are denoted as *All circuit* and experiments with `IBMQJobManager.run` are denoted as *Split jobs*.

5.1 Quantum State Fidelities

We first study quantum state fidelities with respect to the number of CNOT gates required for all Dicke State circuits $Dnk-r$ on different quantum backends. Figure 8 shows measured quantum fidelity of all Dicke States on IBM Q Sydney and IBM Q Montreal system for different transpilation options of IBM QISKIT. Each plot has six lines representing different transpilation techniques and job execution methods outlined in Section 4. The Dicke States are sorted (left to right) according to the number of required CNOT gates in the *untranspiled* circuit. The plots show that for almost all experiments, ‘*Split jobs*’ is equal to or slightly better than ‘*All circuit*’ execution; for these experiments, ‘*Split jobs*’ option has fewer circuits than ‘*All circuit*’ per job.

We present how fidelity changes if we apply measurement error mitigation techniques to the measurement result for each experiment. The left two plots show quantum fidelities on Sydney & Montreal without error mitigation techniques and the right two plots show quantum fidelities after applying error mitigation techniques. We observe that for both Sydney & Montreal, measurement error mitigation reduces noise from the output and increases quantum state fidelities irrespective of circuit length and width.

Theoretically, the number of CNOT count and quantum fidelity measure should have a negative correlation i.e. when CNOT count increases, fidelity measure decreases, and vice versa. We observe that fidelities for Montreal follow this trend for all states with chosen transpilation methods except for state D63-32 where the fidelities are less than state D63-33. From our circuit design, the circuit depth of state D63-33 is (depth = 29) is less than the circuit depth of state D63-32 (depth = 33). So, we can say that reduction in circuit depth increases parallel execution of gates and thus decreases the overall error rate. However, we see from the plot that circuits using default transpilation do not obey this trend for the Montreal backend. We also note that fidelities for Sydney are more distorted especially for noise adaptive transpilation of circuits D41-5, D51-7, D61-9, and D42-10. We investigate the circuit after noise adaptive transpilation and find that the chosen qubits are sometimes not connected which adds more ancilla qubits and thus increases the number of gates. Besides, we find almost similar characteristics for IBM Q Sydney and Montreal using the initial layout provided and default transpiled circuits.

Overall, IBM Q Montreal behaves better with better fidelities than Sydney and there is no irritating ups and down like Sydney. Thus it can be said that the newer system (Montreal) is better and it indeed deserves better Quantum Volume (QV) ranking. Fidelity values of more than 0.5 give us high confidence that the IBMQ devices indeed manage to create entanglement in the Dicke states.

5.2 Influence of Measurement Error Mitigation

To investigate the effect of measurement error mitigation on output, first, we present the absolute difference of quantum fidelities before and after applying error mitigation techniques on IBM Q Sydney & Montreal backend in Figure 9. Similarly, Figure 9 shows the gain of quantum fidelities before and after applying error mitigation techniques on those backends. Six lines are representing different transpilation options and execution methods. All Dicke states denoted using the form $Dnk-r$ are sorted according to number of CNOT gates of

Absolute Difference and Relative Gain of Fidelity for different Dicke States on IBM Q Sydney and Montreal

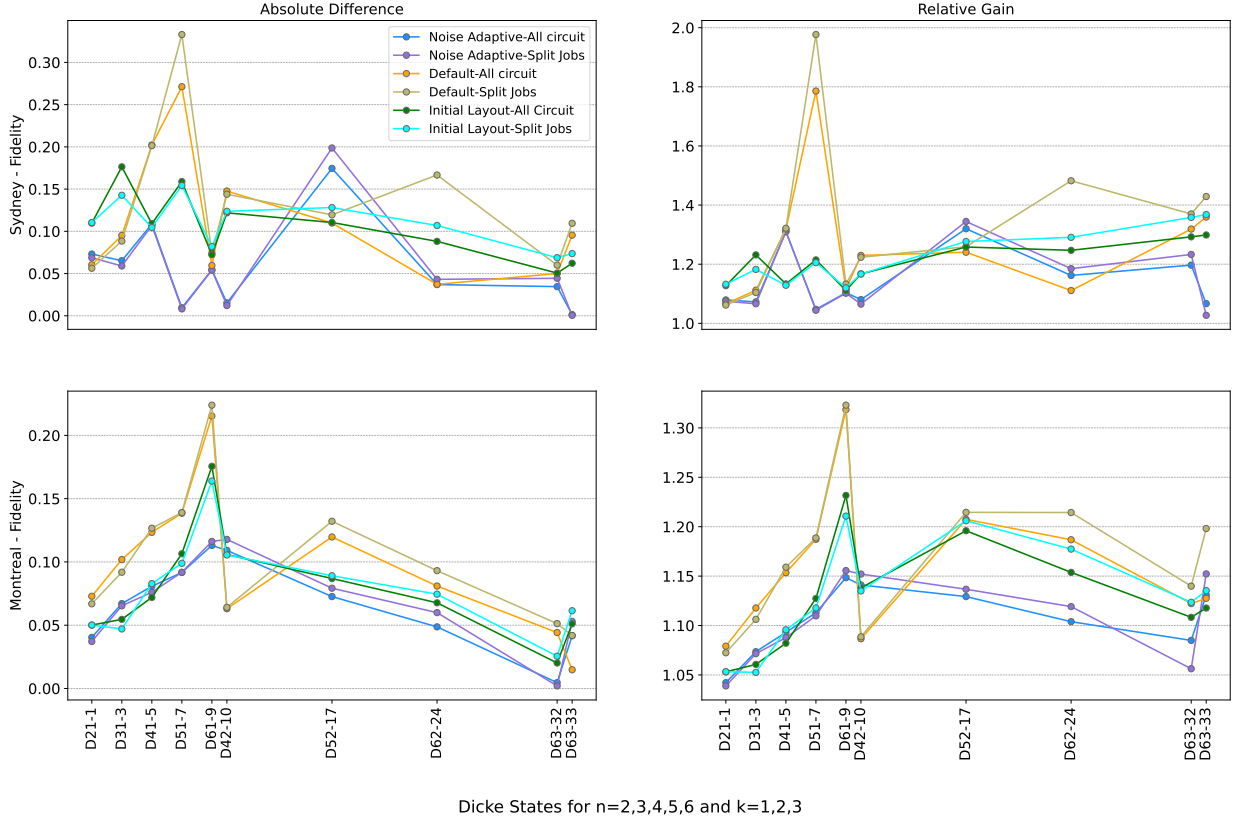


Figure 9: Absolute difference and relative gain of quantum fidelity Dicke States fidelities on IBM Q Sydney (left) and IBM Q Montreal system (right) are measured using different transpilation method of QISKIT with and without applying error mitigation techniques.

untranspiled circuit.

From Figure 9, we observe that in most of the cases, with the increasing number of the qubits, the gain of quantum fidelity increases. Additionally, for the same value of n , fidelity gain is higher for smaller k . This is expected because, for the same n , the higher value of k represents a more complex circuit that has more circuit noise than measurement noise. So, when we apply measurement error mitigation on a less complex circuit (smaller k) for the same n , we get a higher fidelity gain. In general, circuits with an increasing number of qubits get more benefited from measurement error mitigation. For states with the same circuit length, circuit noise dominates over measurement noise in a more complex circuit. However, we observe some exceptions in IBM Q Sydney & Montreal for noise adaptive and initial layout provided transpilation option.

5.3 Info from Classical Distribution

Theoretically, quantum fidelity is upper bounded by the Hellinger fidelity, which in turn is upper bounded by the success probability of output states i.e $Quantum\ Fidelity \leq Hellinger\ Fidelity \leq Measured\ Success\ Probability$. As we discussed before, quantum

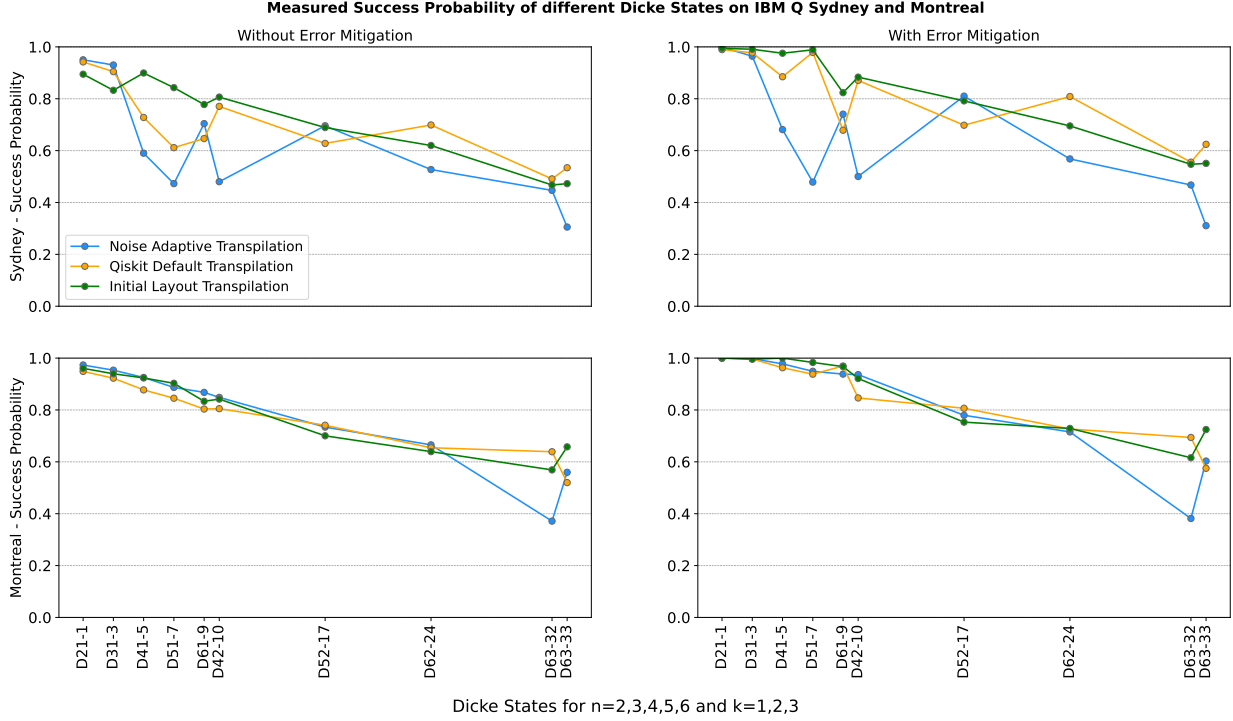


Figure 10: Measured Success Probability of different Dicke States on IBM Q Sydney without error mitigation (top left) & with error mitigation (top right) and on IBM Q Montreal without error mitigation (bottom left) & with error mitigation (bottom right) using QISKIT’s different transpilation with optimization level 3.

fidelity requires 3^n tomography circuits which can be costly and time consuming. Another approach could be to calculate Hellinger fidelity and measured success probability to get an estimation of quantum fidelity of our circuit. In this section, we will explore a comparative study of measured success probability, Hellinger fidelity, and quantum fidelity for our proposed Dicke state preparation circuits. From this section, we only present results from our ‘All Circuit’ execution to avoid complexity.

Figure 10 & 11 shows measured success probability and Hellinger fidelity of different Dicke States on IBM Q Sydney and Montreal backend. We observe that measurement error mitigation increases measured success probability and Hellinger fidelity for both backends. We can find a linear decrease of success rate and Hellinger fidelity in the plot for states sorted (left to right) according to the number of required CNOT gates. However, there are some outlier points in both the plots especially for noise adaptive transpilation on the IBM Q Sydney backend. Recall that noise adaptive transpilation prioritizes error rates for selecting qubits that sometimes choose non-neighboring qubits. This induces overhead of ancilla qubits in the circuit for multi-qubits gates such as CNOT which leads to the lower count of the correct output state. By definition, success probability depends on the number of correct states among a total number of shots, and Hellinger distance is calculated using the probabilities from correct and incorrect states.

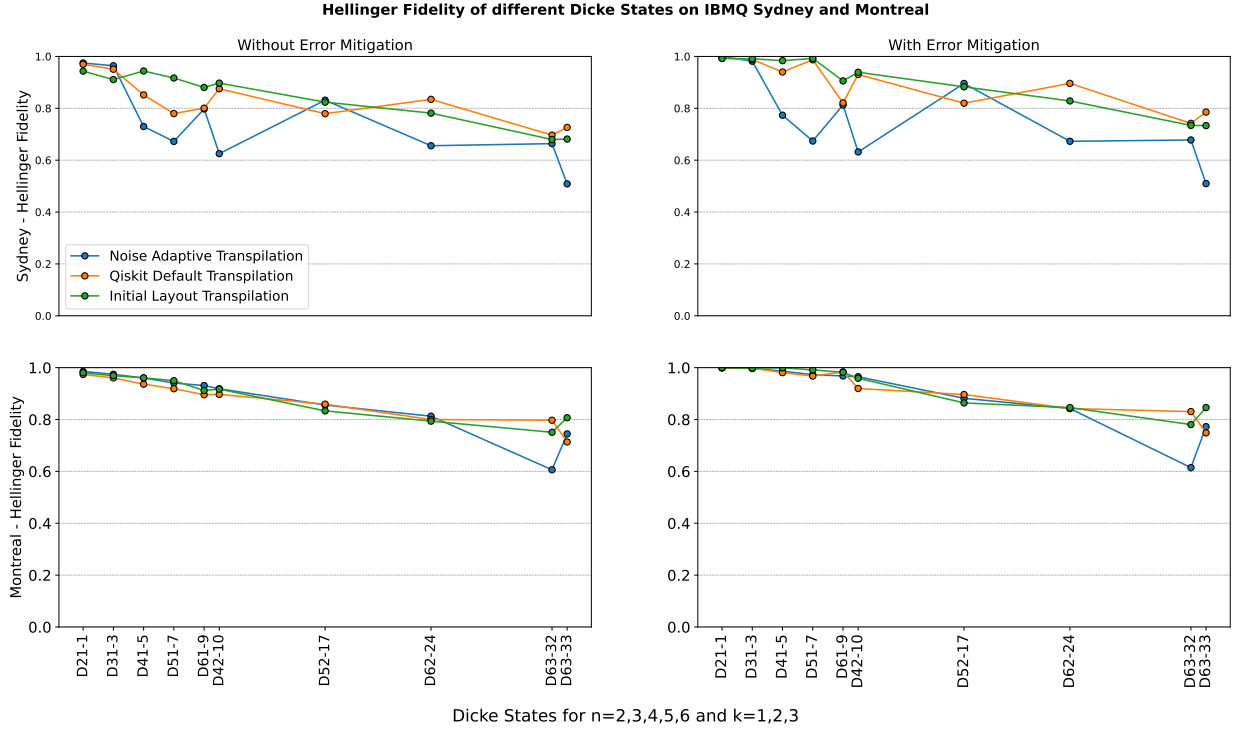


Figure 11: Hellinger fidelity of Dicke States for IBM Q Sydney system without error mitigation (top left) & with error mitigation (top right) and IBM Q Montreal system without error mitigation (bottom left) & with error mitigation (bottom right) using different transpilation method of QISKIT.

In Figure 12, we present all three measures i.e measured success probability, Hellinger fidelity and quantum fidelity for Dicke states D21-1, D31-3, D41-5, D51-7, D61-9, D42-10, D52-17, D62-24, D63-32 and D63-33 using our proposed optimized circuits. We observe that measured success probability is close to Hellinger fidelity for all transpiled circuits on IBM Q Sydney and Montreal. While quantum fidelity is close to the other two measures for the smaller circuits, with increasing circuit length and depth quantum fidelity starts to drop significantly. In summary, we find from our experiment that measured success probability and Hellinger fidelity follows theoretical expectation, and quantum fidelity increases gap with other two measure for a complex circuit. Also, the computationally inexpensive Hellinger fidelity and measured success probability are good approximations for quantum fidelity, particularly up to 4 qubits and 10 CNOTs; unfortunately, the gap becomes larger for larger circuits, but the inexpensive measure still capture all the interesting trends. Note in particular, how Hellinger fidelity replicates the behavior of quantum fidelity for the $|D_3^6\rangle$ inversions under different transpilation schemes.

The measured success probability shown in Figure 10 represents the probability of generating the Dicke States with correct Hamming weight. It would be intriguing to observe the success probabilities of the correct and incorrect Hamming weight of a Dicke States. Figure 13 shows the measured success probability of correct Hamming weight states as well as a boxplot of incorrect Hamming weight states for our proposed Dicke States. For each

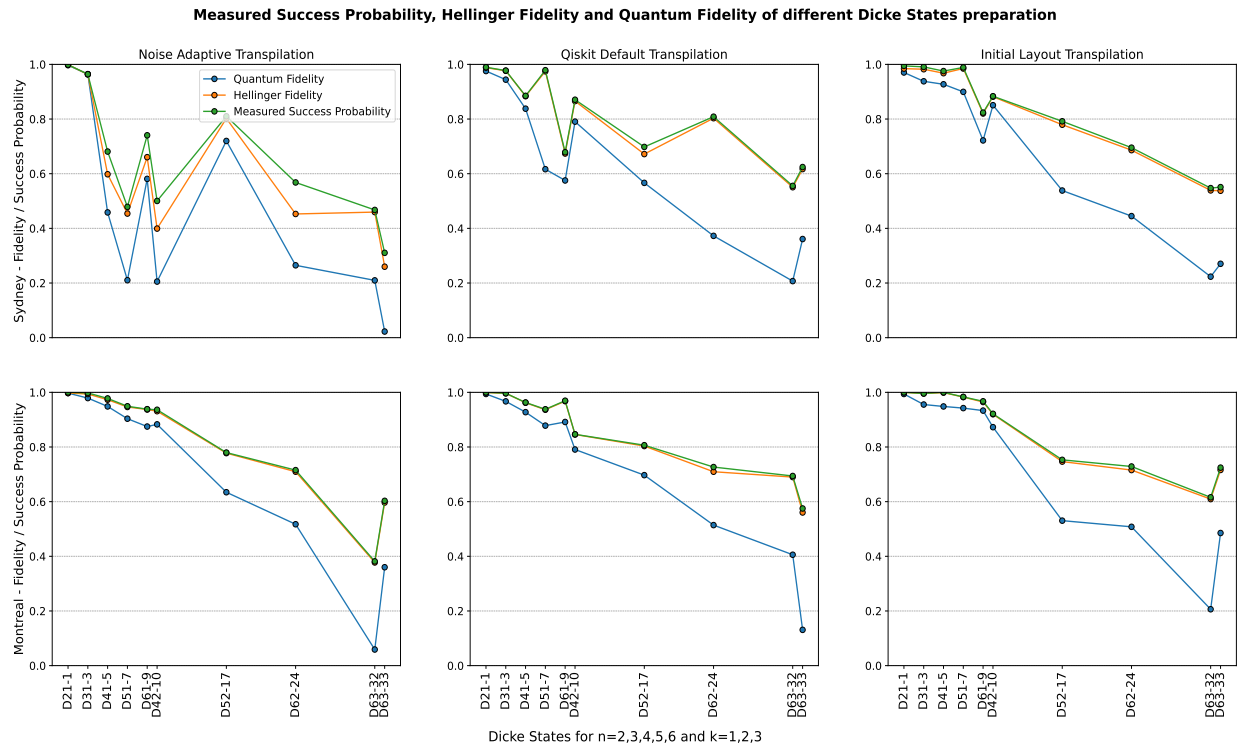


Figure 12: Measured Success Probability, Hellinger Fidelity and Quantum Fidelity of different Dicke States on IBM Q Sydney (upper three) and on IBM Q Montreal (bottom three) with error mitigation using QISKIT’s different transpilation with optimization level 3.

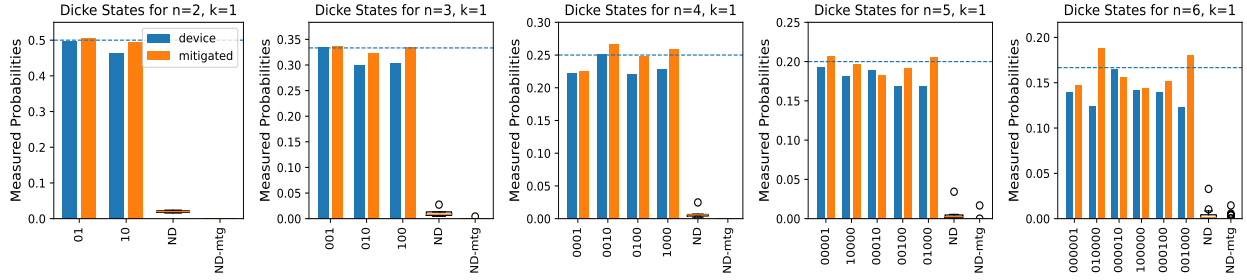
plot, we show both device-generated probabilities and measurement error mitigated probabilities. The horizontal bar in each plot represents the expected probability of correct Hamming weight states i.e. $1/\binom{n}{k}$. We plot the Dicke States with the same Hamming weight ($k = 1, 2, 3$) in a row. For Hamming weight $k = 1$, we see the probabilities of correct Hamming weight to be almost equal to the theoretical expectation while the incorrect Hamming weight states have a small distribution. We find almost similar characteristics for Hamming weight $k = 2$ although the measured probability decreases with increasing n . The success probabilities of correct Hamming weight states for Hamming weight $k = 3$ are much less than the expected probabilities because circuit noise dominates over measurement noise for a complex circuit. However, the probability distribution of incorrect Hamming weight states is still very small. The plots in Figure 13 are totally in line with our results from Figure 10, 11 & 12 and justifies our findings.

6 Conclusion and Outlook

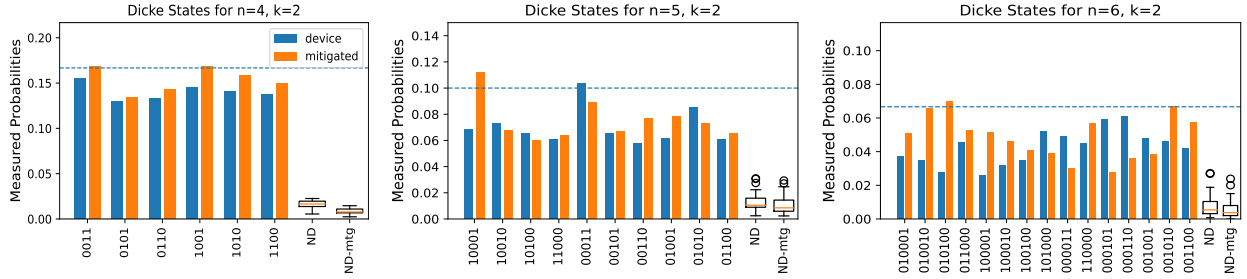
We have presented a new divide-and-conquer-style quantum algorithm for creating Dicke states, which are by definition highly entangled quantum states. Our algorithms leverage the underlying topology of the actual quantum hardware, such as linear nearest neighbor. As an additional theoretical contribution, we showed a bound of how close any product

Success Probabilities of Correct and Incorrect Hamming Weight States for Dicke States ($n = 2, 3, 4, 5, 6$ and $k = 1, 2, 3$)

Hamming weight, $k = 1$:



Hamming weight, $k = 2$:



Hamming weight, $k = 3$:

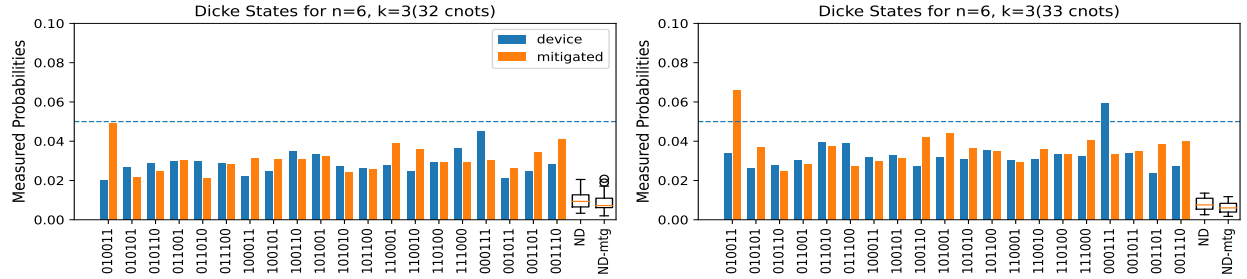


Figure 13: Measured Probability of correct Hamming weights vs. incorrect Hamming weight distribution for Dicke states for $n = 2, 3, 4, 5$ and $k = 1, 2, 3$ using initial layout provided transpilation with optimization level 3. The results are obtained from our experiments in IBM Q Montreal device. Here, 'ND' denotes the distribution of incorrect Hamming weight states (Non-Dicke). The 'blue' bar represents success rate without error mitigation while 'red' bar represents success rate with error mitigation. The horizontal line in each plot shows ideal probability of dicke states with correct Hamming weight.

state can get to a Dicke state in terms of quantum fidelity. Our main experimental results show that present-day NISQ devices (namely two of the IBMQ backends) are indeed able to create Dicke states at very high quantum fidelity levels of more than 0.5 at six qubits, which we verified through full state tomography, thus outperforming previously reported results. This improved performance is due to both improvements in NISQ hardware as well as our algorithmic improvements. In addition, we have examined the suitability of simpler measures of success probability and Hellinger fidelity as approximations for quantum fidelity; we found that these measures match the trends for quantum fidelity. We have also explored the IBM QISKIT software stack with respect to different compiler options and found that no single setting finds the optimum solutions in each case, thus forcing the user to experiment with different settings for their own experiments.

We see the following future directions:

- The cost of the “Divide” part scales well on Ladder architectures but not for LNN architectures. What is the trade-off of the Divide-and-Conquer approach versus architectural constraints? Can we get sub-linear circuit depths $o(n)$ for full connectivity or small constant factors for the CNOT count in LNN connectivities?
- The cost of full state tomography gets prohibitively large even for small $n \geq 6$. Can we approximate ρ and the quantum fidelity from below with fewer tomography circuits in addition to the upper bound given by the Hellinger fidelity?
- The divide-and-conquer approach presented in this paper improved on constants in the running time [3] and on connectivity requirements [26]. To get an asymptotic improvement in the circuit depth, one may recursively apply the divide-and-conquer approach, which is active work in progress [4].
- Dicke states live in the symmetric subspace of the full Hilbert space. By considering the symmetry of Dicke states, there might be more error mitigation potential that can be developed to further improve the fidelity.

References

- [1] Israel F Araujo, Daniel K Park, Francesco Petruccione, and Adenilton J da Silva. A divide-and-conquer algorithm for quantum state preparation. *Scientific Reports*, 11(1):1–12, 2021. [arXiv:2008.01511](#), [doi:10.1038/s41598-021-85474-1](#).
- [2] Dave Bacon, Isaac L. Chuang, and Aram W. Harrow. Efficient Quantum Circuits for Schur and Clebsch-Gordan Transforms. *Physical Review Letters*, 97(17):170502, Oct 2006. [arXiv:quant-ph/0407082](#), [doi:10.1103/PhysRevLett.97.170502](#).
- [3] Andreas Bärtzchi and Stephan Eidenbenz. Deterministic Preparation of Dicke States. In *22nd International Symposium on Fundamentals of Computation Theory, FCT’19*, pages 126–139, 2019. [arXiv:1904.07358](#), [doi:10.1007/978-3-030-25027-0_9](#).
- [4] Andreas Bärtzchi and Stephan Eidenbenz. Short-Depth Circuits for Dicke State Preparation, 2022. In preparation.

- [5] Anil Kumar Bhattacharyya. On a Measure of Divergence between Two Multinomial Populations. *Sankhyā: The Indian Journal of Statistics*, 7(4):401–406, 1946. URL: <http://www.jstor.org/stable/25047882>.
- [6] Andreas Bärtzchi and Stephan Eidenbenz. Grover Mixers for QAOA: Shifting Complexity from Mixer Design to State Preparation. In *IEEE International Conference on Quantum Computing & Engineering QCE'20*, pages 72–82, 2020. [arXiv:2006.00354](https://arxiv.org/abs/2006.00354), [doi:10.1109/QCE49297.2020.00020](https://doi.org/10.1109/QCE49297.2020.00020).
- [7] Andrew M. Childs, Edward Farhi, Jeffrey Goldstone, and Sam Gutmann. Finding cliques by quantum adiabatic evolution. *Quantum Information & Computation*, 2(3):181–191, Apr 2002. [arXiv:quant-ph/0012104](https://arxiv.org/abs/quant-ph/0012104), [doi:10.26421/QIC2.3](https://doi.org/10.26421/QIC2.3).
- [8] I. L. Chuang and D. S. Modha. Reversible arithmetic coding for quantum data compression. *IEEE Transactions on Information Theory*, 46(3):1104–1116, May 2000. [doi:10.1109/18.841192](https://doi.org/10.1109/18.841192).
- [9] Jeremy Cook, Stephan Eidenbenz, and Andreas Bärtzchi. The Quantum Alternating Operator Ansatz on Maximum k-Vertex Cover. In *IEEE International Conference on Quantum Computing & Engineering QCE'20*, pages 83–92, 2020. [arXiv:1910.13483](https://arxiv.org/abs/1910.13483), [doi:10.1109/QCE49297.2020.00021](https://doi.org/10.1109/QCE49297.2020.00021).
- [10] Diogo Cruz, Romain Fournier, Fabien Gremion, Alix Jeannerot, Kenichi Komagata, Tara Tosić, Jarla Thiesbrummel, Chun Lam Chan, Nicolas Macris, Marc-André Dupertuis, and Clément Javerzac-Galy. Efficient Quantum Algorithms for GHZ and W States, and Implementation on the IBM Quantum Computer. *Advanced Quantum Technologies*, 2(5-6):1900015, 2019. [arXiv:1807.05572](https://arxiv.org/abs/1807.05572), [doi:10.1002/qute.201900015](https://doi.org/10.1002/qute.201900015).
- [11] Tiago ML de Veras, Leon D da Silva, and Adenilton J da Silva. Double sparse quantum state preparation. *arXiv preprint arXiv:2108.13527*, 2021. [arXiv:2108.13527](https://arxiv.org/abs/2108.13527).
- [12] R. H. Dicke. Coherence in spontaneous radiation processes. *Physical Review*, 93(1):99–110, Jan 1954. [doi:10.1103/PhysRev.93.99](https://doi.org/10.1103/PhysRev.93.99).
- [13] Craig Gidney. Quirk: Quantum Circuit Simulator. A drag-and-drop quantum circuit simulator. URL: <https://algassert.com/quirk>.
- [14] John Golden, Andreas Bärtzchi, Stephan Eidenbenz, and Daniel O’Malley. Evidence for super-polynomial advantage of qaoa over unstructured search. *arXiv e-prints*, 2022. [arXiv:2202.00648](https://arxiv.org/abs/2202.00648).
- [15] John Golden, Andreas Bärtzchi, Daniel O’Malley, and Stephan Eidenbenz. Threshold-Based Quantum Optimization. In *IEEE International Conference on Quantum Computing & Engineering QCE'21*, pages 137–147, 2021. [arXiv:2106.13860](https://arxiv.org/abs/2106.13860), [doi:10.1109/QCE52317.2021.00030](https://doi.org/10.1109/QCE52317.2021.00030).
- [16] Stuart Hadfield, Zhihui Wang, Bryan O’Gorman, Eleanor G. Rieffel, Davide Venturelli, and Rupak Biswas. From the Quantum Approximate Optimization Algorithm

- to a Quantum Alternating Operator Ansatz. *Algorithms*, 12(2):34, 2019. [arXiv:1709.03489](#), [doi:10.3390/a12020034](#).
- [17] Ernst Hellinger. Neue Begründung der Theorie quadratischer Formen von unendlichvielen Veränderlichen. *Journal für die reine und angewandte Mathematik*, 1909(136):210–271, 1909. [doi:10.1515/crll.1909.136.210](#).
- [18] D. B. Hume, C. W. Chou, T. Rosenband, and D. J. Wineland. Preparation of dicke states in an ion chain. *Physical Review A*, 80(5):052302, Nov 2009. [arXiv:0909.0046](#), [doi:10.1103/PhysRevA.80.052302](#).
- [19] Svetoslav S. Ivanov, Nikolay V. Vitanov, and Natalia V. Korolkova. Creation of arbitrary dicke and NOON states of trapped-ion qubits by global addressing with composite pulses. *New Journal of Physics*, 15(2):023039, Feb 2013. [arXiv:1209.4488](#), [doi:10.1088/1367-2630/15/2/023039](#).
- [20] Daniel F. V. James, Paul G. Kwiat, William J. Munro, and Andrew G. White. Measurement of qubits. *Physical Review A*, 64:052312, 2001. [doi:10.1103/PhysRevA.64.052312](#).
- [21] Mattias T Johnsson, Nabomita Roy Mukty, Daniel Burgarth, Thomas Volz, and Gavin K Brennen. Geometric pathway to scalable quantum sensing. *Physical Review Letters*, 125(19):190403, 2020. [arXiv:1908.01120](#), [doi:10.1103/PhysRevLett.125.190403](#).
- [22] Richard Jozsa. Fidelity for Mixed Quantum States. *Journal of Modern Optics*, 41(12):2315–2323, 1994. [doi:10.1080/09500349414552171](#).
- [23] L. Lamata, C. E. López, B. P. Lanyon, T. Bastin, J. C. Retamal, and E. Solano. Deterministic generation of arbitrary symmetric states and entanglement classes. *Phys. Rev. A*, 87(3):032325, Mar 2013. [arXiv:1211.0404](#), [doi:10.1103/PhysRevA.87.032325](#).
- [24] Emanuel Malvetti, Raban Iten, and Roger Colbeck. Quantum circuits for sparse isometries. *Quantum*, 5:412, 2021. [arXiv:2006.00016v2](#), [doi:10.22331/q-2021-03-15-412](#).
- [25] Michele Mosca and Phillip Kaye. Quantum Networks for Generating Arbitrary Quantum States. In *Optical Fiber Communication Conference and International Conference on Quantum Information ICQI*, page PB28, Jun 2001. [arXiv:quant-ph/0407102](#), [doi:10.1364/ICQI.2001.PB28](#).
- [26] Chandra Sekhar Mukherjee, Subhamoy Maitra, Vineet Gaurav, and Dibyendu Roy. Preparing Dicke States on a Quantum Computer. *IEEE Transactions on Quantum Engineering*, 1:1–17, 2020. [doi:10.1109/TQE.2020.3041479](#).
- [27] Prakash Murali, Jonathan M Baker, Ali Javadi-Abhari, Frederic T Chong, and Margaret Martonosi. Noise-adaptive compiler mappings for noisy intermediate-scale quantum

- computers. In *Proceedings of the Twenty-Fourth International Conference on Architectural Support for Programming Languages and Operating Systems*, pages 1015–1029, 2019. [arXiv:1901.11054](#), [doi:10.1145/3297858.3304075](#).
- [28] Michael A Nielsen and Isaac Chuang. Quantum computation and quantum information, 2002.
- [29] Yingkai Ouyang. Permutation-invariant quantum codes. *Physical Review A*, 90(6):062317, 2014. [arXiv:1302.3247](#), [doi:10.1103/PhysRevA.90.062317](#).
- [30] Yingkai Ouyang. Permutation-invariant quantum coding for quantum deletion channels. In *2021 IEEE International Symposium on Information Theory (ISIT)*, pages 1499–1503. IEEE, 2021. [arXiv:2102.02494](#), [doi:10.1109/ISIT45174.2021.9518078](#).
- [31] Yingkai Ouyang. Quantum storage in quantum ferromagnets. *Physical Review B*, 103(14):144417, 2021. [arXiv:1904.01458](#), [doi:10.1103/PhysRevB.103.144417](#).
- [32] Yingkai Ouyang, Nathan Shettell, and Damian Markham. Robust quantum metrology with explicit symmetric states. *IEEE Transactions on Information Theory*, 2021. [arXiv:1908.02378](#), [doi:10.1109/TIT.2021.3132634](#).
- [33] Martin Plesch and Vladimír Bužek. Efficient compression of quantum information. *Physical Review A*, 81(3):032317, Mar 2010. [arXiv:0907.1764](#), [doi:10.1103/PhysRevA.81.032317](#).
- [34] R. Prevedel, G. Cronenberg, M. S. Tame, M. Paternostro, P. Walther, M. S. Kim, and A. Zeilinger. Experimental Realization of Dicke States of up to Six Qubits for Multiparty Quantum Networking. *Physical Review Letters*, 103(2):020503, Jul 2009. [arXiv:0903.2212](#), [doi:10.1103/PhysRevLett.103.020503](#).
- [35] Qiskit. How does the Qiskit Transpiler Work? URL: <https://medium.com/qiskit/how-does-the-qiskit-transpiler-work-6710863beaac>.
- [36] Qiskit Development Team. Qiskit Documentation: Measurement Error Mitigation. URL: https://qiskit.org/documentation/tutorials/noise/3_measurement_error_mitigation.html.
- [37] Qiskit Development Team. Qiskit Documentation: Quantum Tomography. URL: https://qiskit.org/documentation/tutorials/noise/8_tomography.html.
- [38] Xiao-Qiang Shao Shao, Li Chen, Shou Zhang, Yong-Fang Zhao, and Kyu-Hwang Yeon. Deterministic generation of arbitrary multi-atom symmetric Dicke states by a combination of quantum Zeno dynamics and adiabatic passage. *EPL (Europhysics Letters)*, 90(5):50003, Jun 2010. [doi:10.1209/0295-5075/90/50003](#).
- [39] John K. Stockton, Ramon van Handel, and Hideo Mabuchi. Deterministic Dicke-state preparation with continuous measurement and control. *Physical Review A*, 70(2):022106, Aug 2004. [arXiv:quant-ph/0402137](#), [doi:10.1103/PhysRevA.70.022106](#).

- [40] Géza Tóth. Multipartite entanglement and high-precision metrology. *Physical Review A*, 85(2):022322, Feb 2012. [arXiv:1006.4368](#), [doi:10.1103/PhysRevA.85.022322](#).
- [41] Zhihui Wang, Nicholas C. Rubin, Jason M. Dominy, and Eleanor G. Rieffel. XY mixers: Analytical and numerical results for the quantum alternating operator ansatz. *Physical Review A*, 101(1):012320, 2020. [arXiv:1904.09314](#), [doi:10.1103/PhysRevA.101.012320](#).
- [42] Witlef Wieczorek, Roland Krischek, Nikolai Kiesel, Patrick Michelberger, Géza Tóth, and Harald Weinfurter. Experimental Entanglement of a Six-Photon Symmetric Dicke State. *Physical Review Letters*, 103(2):020504, Jul 2009. [arXiv:0903.2213](#), [doi:10.1103/PhysRevLett.103.020504](#).
- [43] Chunfeng Wu, Chu Guo, Yimin Wang, Gangcheng Wang, Xun-Li Feng, and Jing-Ling Chen. Generation of Dicke states in the ultrastrong-coupling regime of circuit QED systems. *Physical Review A*, 95(1):013845, Jan 2017. [doi:10.1103/PhysRevA.95.013845](#).
- [44] Chunfeng Wu, Yimin Wang, Chu Guo, Yingkai Ouyang, Gangcheng Wang, and Xun-Li Feng. Initializing a permutation-invariant quantum error-correction code. *Physical Review A*, 99(1):012335, 2019. [doi:10.1103/PhysRevA.99.012335](#).
- [45] Yun-Feng Xiao, Xu-Bo Zou, and Guang-Can Guo. Generation of atomic entangled states with selective resonant interaction in cavity quantum electrodynamics. *Physical Review A*, 75(1):012310, Jan 2007. [doi:10.1103/PhysRevA.75.012310](#).
- [46] Xiao-Ming Zhang, Tongyang Li, and Xiao Yuan. Quantum state preparation with optimal circuit depth: Implementations and applications. *arXiv preprint arXiv:2201.11495*, 2022. [arXiv:2201.11495](#).
- [47] Xiao-Ming Zhang, Man-Hong Yung, and Xiao Yuan. Low-depth quantum state preparation. *Physical Review Research*, 3(4):043200, 2021. [arXiv:2102.07533](#), [doi:10.1103/PhysRevResearch.3.043200](#).
- [48] Sahin K. Özdemir, Junichi Shimamura, and Nobuyuki Imoto. A necessary and sufficient condition to play games in quantum mechanical settings. *New Journal of Physics*, 9(2):43–43, Feb 2007. [arXiv:quant-ph/0703006](#), [doi:10.1088/1367-2630/9/2/043](#).